doi.org/10.36721/PJPS.2026.39.12.343.1

miRNA-34b overexpression alleviates neuromyelitis optica spectrum disorders by regulating the TIA-1-stress granule pathway

Yan Dai[1#]*, Anlang Dai[2#] and Yuhuan Liu[1]
[1]Department of Ophthalmology, Lanzhou Petrochemical General Hospital, Lanzhou City, Gansu Province, 730000, China
[2]Department of Anesthesiology, Shenyang Medical College, Shenyang City, Liaoning Province, 110000, China

Abstract: **Background**: Neuromyelitis optica spectrum disorders (NMOSD) are autoimmune demyelinating diseases of the central nervous system. The role of microRNA-34b (miR-34b) in NMOSD pathogenesis remains unclear. This study investigates the expression and functional mechanism of miR-34b in NMOSD, specifically its regulation of the TIA-1-stress granule pathway. **Objectives**: To determine the expression level of miR-34b in NMOSD tissues and cell lines and to elucidate whether miR-34b suppresses cell proliferation and promotes apoptosis by directly targeting the TIA-1-stress granule pathway. **Methods**: Real-time PCR was used to detect miR-34b expression in 25 NMOSD tissue specimens obtained from a hospital laboratory (13 early-stage, 12 chronic-stage) and 10 normal control tissues, as well as in RGC-5 cells. RGC-5 cells were transfected with miR-34b mimics, inhibitors or negative controls. Cell proliferation was assessed by MTT assay and cell cycle distribution and apoptosis was analyzed by flow cytometry (PI staining and Annexin V-FITC/PI double staining, respectively). The direct binding between miR-34b and the 3'-UTR of TIA-1 mRNA was validated using a dual-luciferase reporter assay. Protein expression levels of TIA-1, SG, HuR, CDK2 and BCL-2 were measured by Western blot. A rescue experiment was performed by co-transfecting miR-34b mimics with a TIA-1 overexpression plasmid. **Results**: miR-34b was lower in NMOSD vs controls (0.32 ± 0.08 vs. 1.00 ± 0.12, $P<0.01$), especially in the chronic stage. miR-34b mimics inhibited proliferation, induced G0/G1 arrest (68.5% vs. 52.1%, $P<0.01$) and increased apoptosis (22.6% vs. 8.3%, $P<0.001$). miR-34b inhibitor had opposite effects. miR-34b directly bound TIA-1 3'-UTR and downregulated TIA-1, SG, HuR. TIA-1 overexpression partially reversed miR-34b effects. **Conclusions**: miR-34b is downregulated in NMOSD. Overexpression of miR-34b suppresses proliferation and promotes apoptosis by targeting the TIA-1-stress granule pathway. Restoring miR-34b may be a therapeutic strategy for NMOSD.

Keywords: Apoptosis; Cell proliferation; Cycle arrest; miRNA-34b; Neuromyelitis optica; TIA-1-SG pathway

Submitted on 25-01-2026 – Revised on 09-05-2026 – Accepted on 04-06-2026 – Available online on 26-08-2026 – Published on 01-12-2026

INTRODUCTION

Neuromyelitis optica spectrum disorder (NMOSD) is an autoimmune inflammatory demyelinating disease of the central nervous system that primarily affects the optic nerves and spinal cord (Khadka *et al*., 2022). According to the updated 2015 diagnostic criteria, the majority of NMOSD patients have serum aquaporin-4 (AQP4) antibodies, with an annual incidence of approximately 0.5–4 per 100,000 (Hsu *et al*., 2025). The pathogenesis primarily involves AQP4 antibody-mediated complement-dependent and antibody-dependent cellular cytotoxicity, leading to astrocyte damage, secondary demyelination and axonal injury. Despite advances in immunotherapy, many patients still experience recurrent attacks and accumulate disability, highlighting the urgent need for novel molecular targets and biomarkers.

MicroRNAs (miRNAs) are a class of endogenous, non-coding small RNA molecules approximately 18–24 nucleotides in length that regulate gene expression at the post-transcriptional level by binding to the 3′-untranslated region (3′-UTR) of target mRNAs (Lee *et al*., 2024). Accumulating evidence indicates that multiple miRNAs are involved in the pathogenesis of neuroinflammation and demyelinating diseases (McGurran *et al*., 2026; Ma *et al*., 2024). Among them, the miR-34 family has been reported to regulate apoptosis, autophagy and inflammatory responses in central nervous system disorders. However, the specific role of miRNA-34b in NMOSD remains unclear.

Stress granules are cytoplasmic ribonucleoprotein aggregates formed under stress conditions, exerting protective effects by transiently halting translation and inhibiting apoptosis (Baymiller *et al*., 2026). T-cell intracellular antigen-1 (TIA-1) is a key RNA-binding protein that initiates stress granule formation. Studies have shown that the TIA-1-stress granule axis regulates cell survival under stress conditions (Sarkar *et al*., 2024), but its role in the pathogenesis of NMOSD has not yet been explored.

Given the lack of studies linking miRNA-34b to the TIA-1-stress granule pathway and NMOSD, this study aims to investigate miRNA-34 b expression and its functional role in an NMOSD model and to determine whether miRNA-

**Corresponding author:* e-mail: daiyan19712003@163.com
#These authors contributed equally and are the co-first authors.

34b exerts its effects by targeting the TIA-1-stress granule pathway. It is hypothesized that miRNA-34b may inhibit cell proliferation and promote apoptosis in NMOSD-related cell models by regulating the TIA-1-stress granule pathway, thereby providing a potential therapeutic target for NMOSD.

MATERIALS AND METHODS

Tissue specimen collection from hospital laboratory

Tissue specimens were obtained from the laboratory repository of Lanzhou Petrochemical General Hospital, which collected samples from patients diagnosed with NMOSD based on the following criteria: (1) meeting the 2018 international diagnostic criteria for NMOSD (McCreary *et al*., 2018); (2) positive serum AQP4 antibodies; (3) first attack and no prior immunotherapy. Exclusion criteria applied during sample collection included: (1) coexistence of other autoimmune diseases; (2) concomitant central nervous system infection or tumor; (3) pregnancy or lactation; (4) recent use of immunomodulatory agents.

A total of 25 NMOSD tissue specimens were obtained from the laboratory, including 13 from early-stage (disease duration <1 year) and 12 from chronic-stage (disease duration ≥2 years). Normal control tissue specimens were obtained from the same laboratory repository and derived from patients undergoing optic nerve resection for ocular trauma during the same period (n=10). The resected distal normal optic nerve tissue showed no inflammation, demyelination, or gliosis on hematoxylin and eosin (HE) staining. The two groups were matched for age and sex ($P > 0.05$).

Tissue collection and preservation

NMOSD tissue specimens were obtained from the marginal area of lesions (<0.5 cm from the lesion) during diagnostic stereotactic biopsy or decompression surgery. Normal control tissues were obtained from optic nerve stumps of individuals with ocular trauma. All tissues were immediately divided into two parts after excision: one part was snap-frozen in liquid nitrogen and transferred to a -80°C freezer for RNA and protein extraction (Kanai *et al*., 2018); the other part was fixed in 4% paraformaldehyde and embedded in paraffin for pathological confirmation (Shao *et al*., 2017).

Cell culture and passage

This study used the RGC-5 cell line (mouse retinal ganglion cell-like cells) purchased from ScienCell Research Laboratories, USA (Catalog No.: SC-1435). RGC-5 cells were cultured as described previously (Krishnamoorthy *et al*., 2001). Cells were cultured in RPMI-1640 medium containing 10% fetal bovine serum (FBS, Gibco, USA) and 1% penicillin-streptomycin (100 U/mL) in a humidified incubator at 37°C with 5% CO_2. The medium was changed every 2-3 days. When cell confluence reached 80%-90%, the medium was discarded, cells were washed once with PBS and 0.25% trypsin-EDTA was added for 2-3 minutes of digestion. An equal volume of medium containing serum was added to terminate digestion, followed by centrifugation at 1000 rpm for 5 minutes. The supernatant was discarded and cells were resuspended and passaged at a 1:3 ratio. All experiments were performed using cells at passages 5-10. It should be noted that RGC-5 cells cannot fully recapitulate the pathological processes of astrocytes or oligodendrocytes in NMOSD. This study used them only as a neuronal cell model for preliminary mechanistic exploration.

Transfection and transfection efficiency validation

Lipofectamine 2000 was used for cell transfection as described previously (Dalby *et al*., 2004). Twenty-four hours before transfection, RGC-5 cells were seeded into 6-well plates at a density of 1×10^5 cells/well and cultured in RPMI-1640 medium containing 10% FBS, so that cell confluence reached 60%-80% at the time of transfection. Transfection was performed using Lipofectamine 2000 (Invitrogen, USA) according to the manufacturer's instructions. Groups included: miRNA-34b mimic group (50 nM), mimic negative control group (NC mimics), miRNA-34b inhibitor group (50 nM) and inhibitor negative control group (NC inhibitor). Cells were collected 48 hours after transfection for subsequent RNA/protein extraction and functional assays. The sequence of the miRNA-34b mimic was: 5'-UGGUAUCCCAUUUUGGUGA-3'; the inhibitor was the reverse complementary sequence.

Transfection efficiency was validated as follows: 24 hours after transfection, a portion of cells was collected for RNA extraction, and the expression change in miRNA-34b was detected by qPCR. The NC group was used as a control to calculate the relative expression level of miRNA-34b. Efficiency criteria: an increase in expression level of ≥5-fold in the mimics group and a decrease of ≥70% in the inhibitor group were considered successful transfection. Only samples meeting the transfection efficiency criteria were included in subsequent experiments.

Real-time quantitative PCR detection of miRNA-34b expression

Twenty-four hours after transfection, total RNA was extracted using the TRIzol method (Zeng *et al*., 2024). One microgram of RNA was used to synthesize cDNA using a miRNA reverse transcription kit (containing stem-loop primers) or an mRNA reverse transcription kit. The qPCR reaction system (20 μL) consisted of: 10 μL SYBR Green Master Mix, 0.5 μL each of forward and reverse primers (10 μM), 2 μL cDNA template and 7 μL ddH_2O. Reaction conditions were: 95°C for 2 min for initial denaturation; then 40 cycles of 95°C for 15 s (denaturation), 60°C for 30 s (annealing) and 72°C for 30

s (extension) and followed by melting curve analysis (60-95°C, reading every 0.5°C) after the cycles. Each sample was run in triplicate. The relative expression levels of miRNA-34b or TIA-1 mRNA were calculated using the $2^{-\Delta\Delta Ct}$ method, with U6 or GAPDH as internal controls. The qPCR primer sequences were as follows: miRNA-34b forward: 5'-UAGGCAGUGUCAUUAGCUGAUUG-3', the universal reverse primer was provided with the kit; U6 forward: 5'-CTCGCTTCGGCAGCACA-3', reverse: 5'-AACGCTTCACGAATTTGCGT-3'; TIA-1 mRNA forward: 5'-AACGUGCCGUUUAAACCACU-3', reverse: 5'-CAGGCUCAGCUUCUGGAAAU-3'; GAPDH forward: 5'-GGAGCGAGATCCCTCCAAAAT-3', reverse: 5'-GGCTGTTGTCATACTTCTCATGG-3'.

Western blot detection of protein expression

48 hours after transfection, total protein was extracted using RIPA lysis buffer (containing protease inhibitors), and protein concentration was quantified using the BCA method as previously described (Lu *et al*., 2024). Thirty micrograms of protein were mixed with 5× loading buffer and denatured at 95°C for 10 minutes. Proteins were separated by electrophoresis using 10% SDS-PAGE gels (80 V for the stacking gel, 120 V for the resolving gel). Proteins were then transferred onto PVDF membranes using a wet transfer system (300 mA, 90 minutes). After transfer, the membranes were blocked with 5% non-fat milk (dissolved in TBST) for 1 hour at room temperature. The membranes were then incubated with the following primary antibodies (all diluted 1:1000 in primary antibody dilution buffer): TIA-1 (Abcam, ab40693), SG (Abcam, ab108615), HuR (Abcam, ab200342), CKD2 (Abcam, ab32117), BCL-2 (Abcam, ab182858) and GAPDH (Abcam, ab8245). Incubation was carried out overnight (12-16 hours) at 4°C. The next day, the membranes were washed three times with TBST (10 minutes each wash), followed by incubation with HRP-conjugated secondary antibodies (diluted 1:5000 in TBST) for 1 hour at room temperature. After three additional washes with TBST (10 minutes each), protein bands were visualized with an ECL chemiluminescent substrate, and images were captured with a ChemiDoc imaging system. Band gray values were analyzed using ImageJ software. To control for variations in protein loading and transfer, total protein was normalized using Ponceau S staining of the membrane prior to blocking, and the resulting signal was used to calculate a normalization factor for each lane. Alternatively, GAPDH was used as a loading control and its stability across all samples was confirmed by demonstrating no significant difference in GAPDH signal intensity between groups ($P > 0.05$). The relative protein expression level of each target was calculated as the ratio of the target protein's normalized intensity to that of the loading control (total protein or GAPDH).

MTT detecting cell proliferation after transfection

Cell proliferation was detected by referring to previous literature (Mosmann, 1983). At 0, 24, 48, and 72 hours after transfection, 20 μL of MTT solution (5 mg/mL) was added to each well, and the cells were incubated for an additional 4 hours. The supernatant was aspirated and 150 μL of DMSO was added to each well, followed by shaking for 10 minutes to dissolve the formazan crystals. The absorbance was measured at 570 nm using a microplate reader. A cell growth curve was plotted with time on the x-axis and absorbance on the y-axis.

Flow cytometry detecting cell cycle changes

At 24 hours after transfection, cells were collected and washed twice with pre-chilled PBS. One milliliter of pre-chilled 70% ethanol was slowly added and the cells were gently mixed and fixed overnight (12-16 hours) at 4°C. After fixation, the cells were centrifuged at 1000 rpm for 5 minutes, the ethanol was discarded and the cells were washed once with PBS. RNase A (100 μg/mL) was added and the cells were incubated in a 37°C water bath for 30 minutes to remove RNA. Propidium iodide (PI, 50 μg/mL) was then added and the cells were stained for 30 minutes at room temperature in the dark. The method for detecting cell cycle by PI staining was performed according to the relevant literature (Nicoletti *et al*., 1991). PI fluorescence intensity, which is proportional to DNA content, was detected using a BD FACSCalibur flow cytometer (excitation wavelength 488 nm, emission wavelength 585 nm). A total of 20,000 cells were collected per sample and cell cycle distribution was analyzed using ModFit LT 4.0 software. The proportions of cells in the G0/G1, S and G2/M phases were calculated. Cell cycle arrest was defined as a significant increase in the proportion of cells in the G0/G1 phase.

Annexin V-FITC/PI double staining detecting cell apoptosis

According to previous literature, cell apoptosis was detected (Vermes *et al*., 1995). At 48 hours after transfection, cells (including floating cells) were collected, washed twice with pre-chilled PBS and centrifuged at 1000 rpm for 5 minutes. The cells were resuspended in 500 μL of 1× Binding Buffer to adjust the cell density to 1×10^5 cells/mL. Five microliters of Annexin V-FITC and 5 μL of PI (both from an apoptosis detection kit, BD Biosciences) were added, gently mixed and incubated for 15 minutes at room temperature in the dark. After incubation, the samples were analyzed within 1 hour using a BD FACSCalibur flow cytometer with an excitation wavelength of 488 nm; FITC was detected at 530 nm and PI at 585 nm. A total of 10,000 cells were collected per sample and data were analyzed using CellQuest Pro software. Cells were classified into four quadrants: lower left (Annexin V-/PI-, live cells), lower right (Annexin V+/PI-, early apoptotic), upper right (Annexin V+/PI+, late apoptotic/necrotic) and upper left (Annexin V-/PI+, necrotic). According to the relevant literature (Ramedani *et al*., 2023), the apoptosis rate

equals the early apoptosis rate plus the late apoptosis rate.

Dual-luciferase reporter assay validating the targeting relationship

The detection methods refer to the previous literature (Jin *et al*., 2013). Luciferase reporter plasmids containing the wild-type or mutant 3'-UTR of the TIA-1 gene were constructed. RGC-5 cells were seeded into 24-well plates and co-transfected with miRNA-34b mimics or NC mimics along with the reporter plasmids (containing either the wild-type or mutant 3'-UTR). At 48 hours after transfection, firefly luciferase and Renilla luciferase activities were detected using a dual-luciferase reporter assay kit and the relative luciferase activity (firefly/Renilla) was calculated. Bioinformatics predictions were performed using TargetScan 7.2 and miRDB online databases. The prediction results showed a potential binding site (position: 235-241) between miRNA-34b and the TIA-1 mRNA 3'-UTR, with a binding energy of -18.6 kcal/mol and a context++ score of -0.21.

TIA-1 overexpression rescue experiment

To verify whether miRNA-34b exerts its effects through TIA-1, the following groups were established: NC mimics + empty vector, miRNA-34b mimics + empty vector and miRNA-34b mimics + pcDNA3.1-TIA-1. At 48 hours after transfection, cell proliferation (MTT), apoptosis (Annexin V/PI) and cell cycle (PI staining) were detected.

Experimental replicates

To ensure rigor and reproducibility, three independent biological replicates were performed for all experiments. A biological replicate was defined as an independent cell culture passage and transfection event conducted on a different day. For each biological replicate, technical triplicates were included for each experimental condition in assays such as qPCR, MTT and flow cytometry. Data presented in the fgures represent the mean ± standard deviation (SD) calculated from the three biological replicates.

Statistical analysis

Statistical analysis was performed using SPSS 20.0 software. Comparisons between two groups were conducted using the independent samples t-test. Comparisons among multiple groups were performed using one-way analysis of variance (ANOVA), followed by Tukey's post hoc test for pairwise comparisons. For multiple comparisons, the Bonferroni method was used for correction and a corrected P-value (adj. P) < 0.05 was considered statistically significant. All data distributions were confirmed to be normal by the Shapiro-Wilk test. A P-value < 0.05 was considered statistically significant.

RESULTS

Low expression of miRNA-34b in NMOSD

Real-time quantitative PCR results showed that, compared with normal tissues, the relative expression level of miRNA-34b in NMOSD lesional tissues was significantly decreased (0.32 ± 0.08 vs. 1.00 ± 0.12, P < 0.01, Fig. 1A). Further analysis revealed that the expression level of miRNA-34b in tissues from chronic-stage NMOSD (disease duration ≥2 years) was significantly lower than that in early-stage (disease duration <1 year) (0.18 ± 0.05 vs. 0.45 ± 0.09, P < 0.05, Fig. 1B).

Inhibitory effect of miRNA-34b on cell proliferation in neuromyelitis optica

After transfection, the expression level of miRNA-34b in the miRNA-34b mimics group was increased by 6.8-fold compared with the negative control (NC mimics) group (P < 0.001), while the expression level in the miRNA-34b inhibitor group was decreased by 82% (P < 0.01), indicating good overexpression and knockdown efficiency (Figs. 2A, 2B).

MTT assay results showed that, compared with the NC mimics group, cell proliferation viability in the miRNA-34b mimics group was significantly reduced at 48 and 72 hours post-transfection (48h inhibition rate: 35.2% ± 4.1%, P < 0.01; 72h inhibition rate: 48.6% ± 5.3%, P < 0.001). Conversely, compared with the NC inhibitor group, cell proliferation viability in the miRNA-34b inhibitor group was significantly increased at 48 and 72 hours (48h promotion rate: 28.7% ± 3.5%, P < 0.05; 72h promotion rate: 41.5% ± 4.8%, P < 0.01). These results indicate that miRNA-34b can significantly inhibit the proliferation capacity of NMOSD-related cells (Figs. 2C, 2D).

Regulatory effects of miRNA-34b on cell cycle and apoptosis in neuromyelitis optica

Flow cytometry analysis of cell cycle distribution revealed that, compared with the NC mimics group, the proportion of cells in the G0/G1 phase was significantly increased in the miRNA-34b mimics group (P < 0.01), while the proportions of cells in the S and G2/M phases were correspondingly reduced, indicating G0/G1 phase arrest. In contrast, the proportion of cells in the G0/G1 phase in the miRNA-34b inhibitor group was significantly lower than that in the NC inhibitor group (P < 0.05), with accelerated cell cycle progression (Figs. 3A, 3B).

Annexin V-FITC/PI double staining results showed that the total apoptosis rate (early + late) in the miRNA-34b mimics group was significantly higher than that in the NC mimics group (22.6% ± 2.8% vs. 8.3% ± 1.5%, P < 0.001); while the total apoptosis rate in the miRNA-34b inhibitor group was significantly lower than that in the NC inhibitor group (P < 0.05) (Figs. 3C, 3D).

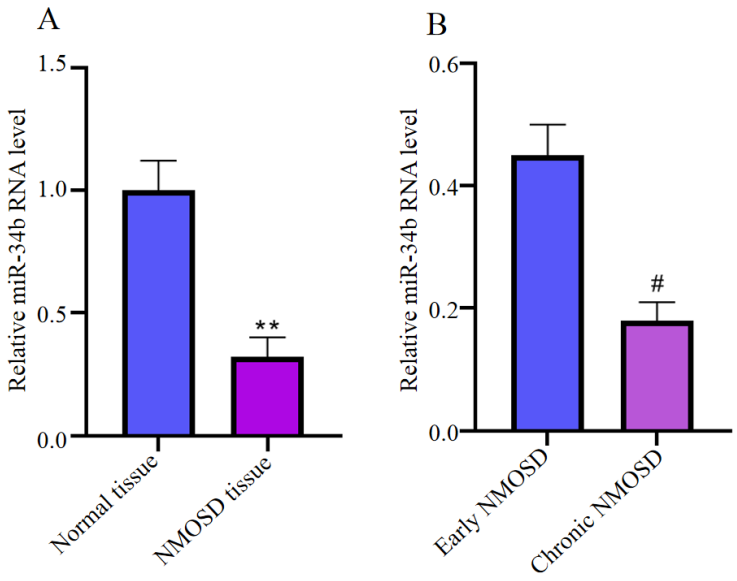

Fig. 1: Low expression of miRNA-34b in NMOSD

(A) Real-time quantitative PCR detection of miRNA-34b expression in NMOSD tissues. NMOSD tissues (n=25), normal control tissues (n=10); (B) Comparison of miRNA-34b expression in NMOSD tissues at different disease stages. Chronic-stage NMOSD (n=12, disease duration ⩾2 years), early-stage (n=13, disease duration <1 year). Data are presented as mean ± standard deviation. **P < 0.01 vs. Normal tissue; #P < 0.05 vs. Early tissue.

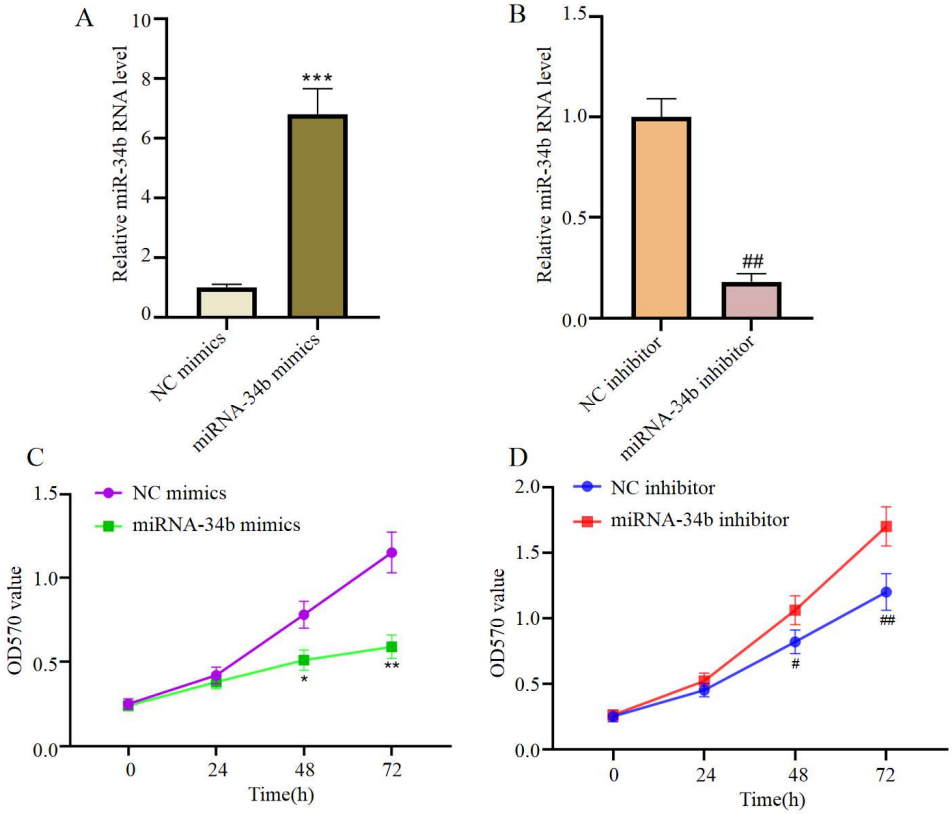

Fig. 2: miRNA-34b inhibiting proliferation of NMOSD cells

(A) Real-time quantitative PCR validation of transfection efficiency of miRNA-34b mimics; (B) Real-time quantitative PCR validation of transfection efficiency of miRNA-34b inhibitor; (C) MTT assay detecting the effect of miRNA-34b mimics on RGC-5 cell proliferation; (D) MTT assay detecting the effect of miRNA-34b inhibitor on RGC-5 cell proliferation. Data are presented as mean ± standard deviation from three independent experiments. *P < 0.05, **P < 0.01 vs. NC mimics; #P < 0.05, ##P < 0.01 vs. NC inhibitor.

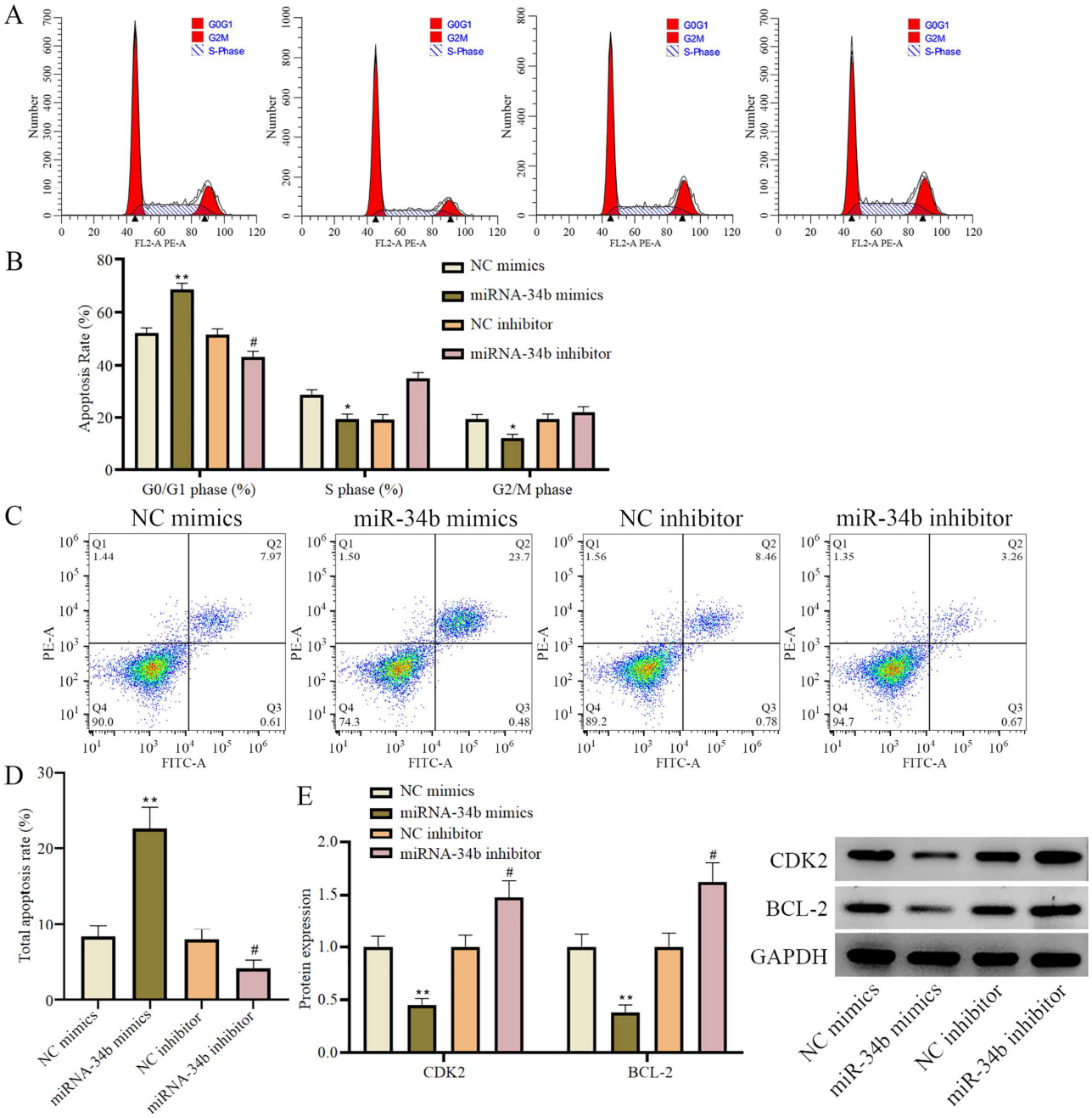

Fig. 3: miRNA-34b promotes apoptosis and cell cycle arrest in neuromyelitis optica cells.
(A) Flow cytometry detecting the effect of miRNA-34b mimics on the cell cycle distribution of RGC-5 cells; (B) Quantitative analysis of cell cycle distribution; (C) Annexin V-FITC/PI double staining detecting the effect of miRNA-34b mimics on apoptosis of RGC-5 cells; (D) Quantitative analysis of apoptosis rate; (E) Western blot detecting the effect of miRNA-34b on the protein expression of CDK2 and BCL-2 in RGC-5 cells. Data are presented as mean ± standard deviation from three independent experiments. **P < 0.01 vs. NC mimics; #P < 0.05 vs. NC inhibitor.

Western blot results showed that, compared with the NC mimics group, the expression levels of the cell cycle-related protein CDK2 and the anti-apoptotic protein BCL-2 were significantly decreased in the miRNA-34b mimics group (P < 0.01). Conversely, the expression levels of CDK2 and BCL-2 in the miRNA-34b inhibitor group were significantly higher than those in the NC inhibitor group (Fig. 3E). These results consistently demonstrate that miRNA-34b promotes apoptosis and induces G0/G1 phase arrest in NMOSD cells.

miRNA-34b regulates the protein expression of key components of the TIA-1-SG pathway

Bioinformatics prediction revealed a potential binding site

between miRNA-34b and the 3'-UTR region of TIA-1 mRNA (Fig. 4A). Dual-luciferase reporter assay confirmed that, compared with the NC mimics co-transfection group, luciferase activity was significantly reduced in the group co-transfected with miRNA-34b mimics and the wild-type TIA-1 3'-UTR vector (relative activity: 0.42 ± 0.05 vs. 1.00 ± 0.09, $P < 0.01$); whereas luciferase activity was not significantly affected after co-transfection with the mutant vector (Fig. 4B). These results indicate that miRNA-34b directly targets and binds to the 3'-UTR of TIA-1 mRNA.

Western blot results showed that, in RGC-5 cells, compared with the NC mimics group, the expression levels of TIA-1 and its downstream stress granule marker protein SG and RNA-binding protein HuR were significantly decreased in the miRNA-34b mimics group. Conversely, the expression levels of the above proteins were significantly increased in the miRNA-34b inhibitor group (Figs. 4C-F). These data demonstrate that miRNA-34b negatively regulates the protein expression levels of TIA-1, SG and HuR, which are key molecular components of the stress granule machinery.

TIA-1 overexpression partially reverses the function of miRNA-34b

The results showed that in RGC-5 cells, transfection with miRNA-34b mimics led to decreased cell proliferation, increased apoptosis and G0/G1 phase arrest. However, when cells were co-transfected with miRNA-34b mimics and a TIA-1 overexpression plasmid (pcDNA3.1-TIA-1), compared with the miRNA-34b mimics-only group, cell proliferation viability was partially restored at 72 hours (0.58 ± 0.06 vs. 0.42 ± 0.04, $P < 0.05$), the apoptosis rate was significantly decreased (15.1% ± 1.9% vs. 23.8% ± 2.5%, $P < 0.01$) and the proportion of cells in the G0/G1 phase was also significantly reduced (59.8% ± 2.1% vs. 69.2% ± 2.4%, $P < 0.05$) (Figs. 5A-C). These results confirm that TIA-1 is a key downstream effector of miRNA-34b and that TIA-1 overexpression can partially antagonize the proliferation-inhibitory and pro-apoptotic effects of miRNA-34b in NMOSD cells.

DISCUSSION

This study is the first to investigate miRNA-34b expression in a cellular model of NMOSD and its regulatory relationship with the TIA-1-stress granule pathway. The results showed that the expression level of miRNA-34b in NMOSD lesional tissues was significantly lower than that in normal control tissues, and was even lower in chronic-stage tissues than in early-stage tissues. This is consistent with previous findings in other central nervous system disorders (Han *et al*., 2023; Mohamed *et al*., 2023). However, direct evidence of changes in miRNA-34b expression in NMOSD is reported here for the first time. It should be noted that the sample size of NMOSD tissues in this study was small (n=25) and the normal controls were obtained from individuals with ocular trauma rather than healthy volunteers, which may introduce selection bias. This is one limitation of this study.

Lack of direct evidence for functional stress granule formation. A critical gap in this study is the absence of direct visualization and quantification of stress granule dynamics. Stress granules are dynamic, microscopically visible ribonucleoprotein aggregates; their formation, size, number, and dissolution cannot be fully inferred from Western blotting of core marker proteins such as TIA-1 or SG. While it is observed that miR-34b modulates TIA-1 and SG protein levels, immunofluorescence (IF) co-localization (e.g., TIA-1/eIF3 or G3BP1) was not done to directly confirm that these changes translate into altered SG formation under cellular stress conditions relevant to NMOSD. It remains possible that miR-34b affects other TIA-1 functions unrelated to SG, or that changes in SG protein levels do not linearly correlate with SG assembly capacity. Future studies must incorporate quantitative IF-based SG assays in appropriate cell models under stress (e.g., arsenite or AQP4-IgG/complement treatment) to establish a direct link between miR-34b, SG formation and cell fate in NMOSD pathophysiology.

Functional experiments in this study demonstrated that overexpression of miRNA-34b significantly inhibited the proliferation and viability of RGC-5 cells, induced G0/G1 phase arrest and promoted cell apoptosis, whereas inhibition of miRNA-34b produced opposite effects. Previous studies have shown that miR-34a inhibits breast cancer stem cell proliferation and chemoresistance by targeting NOTCH1 (Sahin *et al*., 2025); a meta-analysis also supported the association between miR-34b/c polymorphisms and cancer risk (Liu *et al*., 2025). However, the above studies focus on tumor biology, whereas NMOSD is an autoimmune demyelinating disease whose core pathological process involves AQP4 antibody-mediated astrocyte damage rather than the autonomous proliferation of neurons or ganglion cells. The RGC-5 cell line (mouse retinal ganglion cell-like cells) used in this study cannot fully simulate the pathological characteristics of astrocytes or oligodendrocytes in NMOSD, which is another important limitation of this study. RGC-5 cells have been reported to exhibit multiple phenotypic instabilities; therefore, the conclusions of this study need to be validated in more relevant cell models, such as astrocytic cell lines or primary astrocytes.

In this study, the dual-luciferase reporter assay confirmed that miRNA-34b directly targets the 3'-UTR of TIA-1 mRNA and Western blotting showed that miRNA-34b negatively regulates the protein expression of TIA-1, SG and HuR.

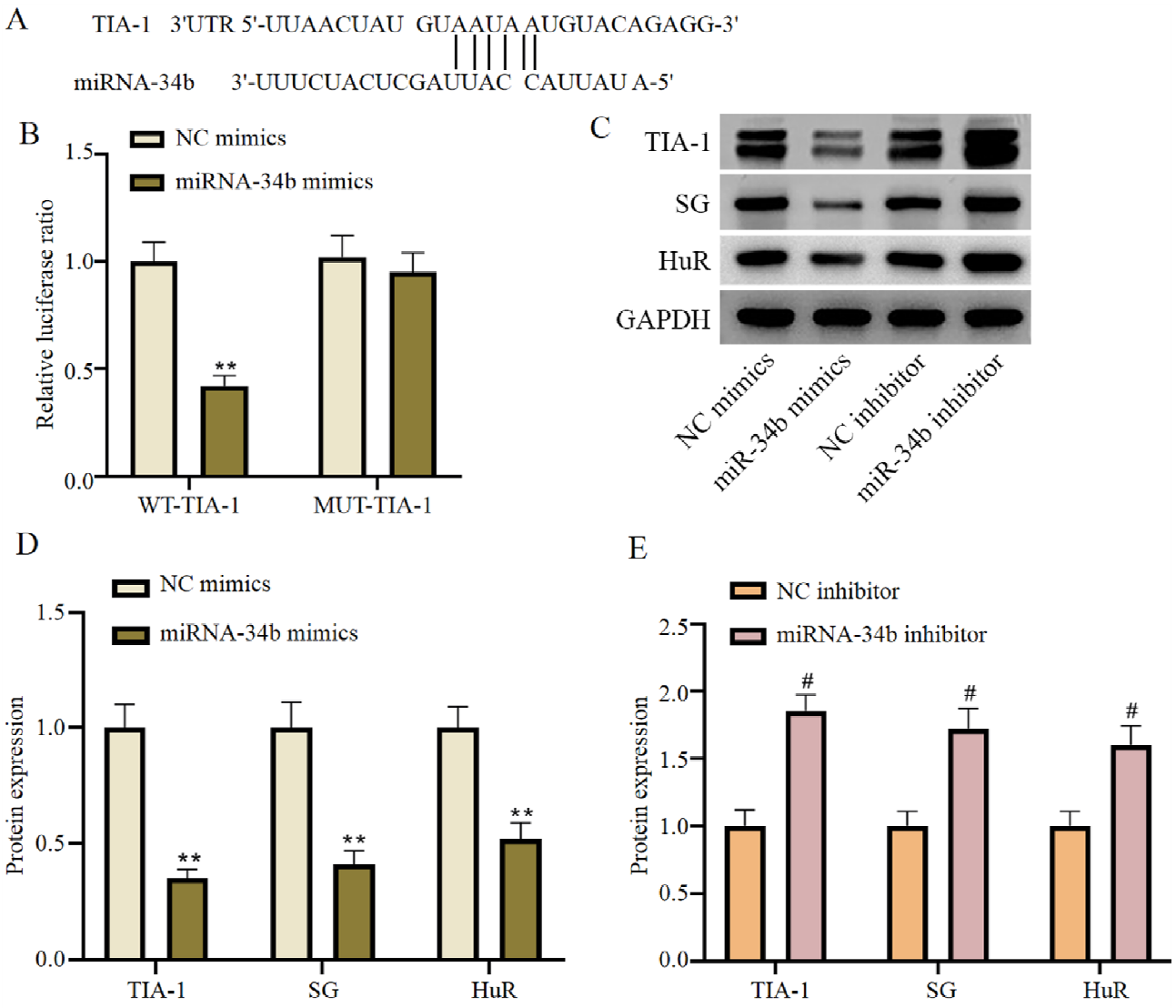

Fig. 4: miRNA-34b participates in the pathogenesis of neuromyelitis optica by targeting the TIA-1-SG pathway. (A) Bioinformatics prediction of the binding site between miRNA-34b and the TIA-1 mRNA 3'-UTR; (B) Dual-luciferase reporter assay validating the targeted binding of miRNA-34b to the TIA-1 3'-UTR. **P < 0.01 vs. NC mimics + WT; (C) Western blot detecting the effect of miRNA-34b on the protein expression of TIA-1, SG, and HuR in RGC-5 cells; (D) Quantitative analysis of TIA-1, SG and HuR protein expression levels in RGC-5 cells. **P < 0.01 vs. NC mimics; (E) Quantitative analysis of TIA-1, SG and HuR protein expression levels in RGC-5 cells. #P < 0.05 vs. NC inhibitor. Data are presented as mean ± standard deviation from three independent experiments.

TIA-1 is a core initiating protein of stress granule formation, which transiently halts translation and inhibits apoptosis by sequestering mRNA under stress conditions (Liu *et al*., 2026; Lesniczak-Staszak *et al*., 2024). Previous studies have also elucidated the recognition and binding mechanisms of TIA-1 to target oligonucleotides. This study found that miRNA-34b promotes cell apoptosis by downregulating the TIA-1-SG pathway, consistent with previous reports showing that stress granules prevent apoptosis by inhibiting mTORC1 signaling (Naki *et al*., 2022; Jiao *et al*., 2024). However, it should be noted that this study did not directly measure stress granule formation by immunofluorescence co-localization but only detected the expression levels of TIA-1 and SG proteins by Western blotting, which cannot be fully equated with the functional activity of stress granules. Furthermore, overexpression of TIA-1 in the rescue experiment only partially reversed the effects of miRNA-34b mimics, suggesting that other downstream targets of miRNA-34b may be involved in its regulation. In fact, bioinformatics predictions indicate that miRNA-34b may target multiple genes involved in cell cycle and apoptosis (Przybyszewski et al., 2024; Ranga et al., 2023), and the observed changes in CDK2 and BCL-2 expression by Western blotting in this study also support this possibility.

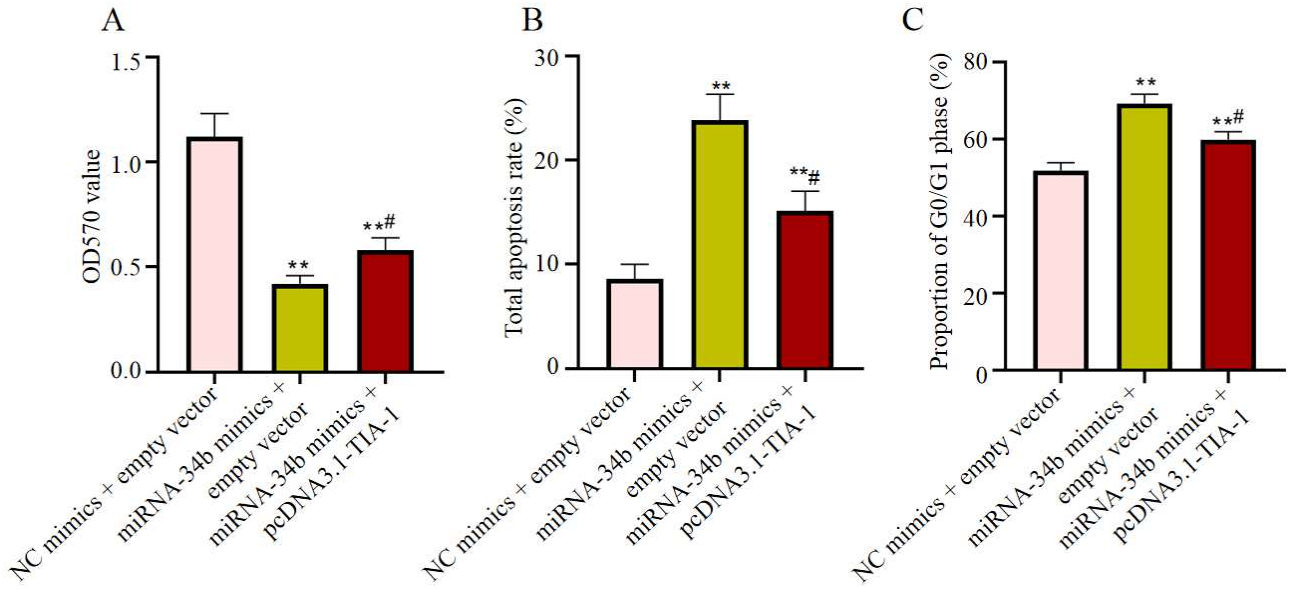

Fig. 5: Overexpression of TIA-1 partially reverses the function of miRNA-34b.
(A) MTT assay detecting the reversal effect of TIA-1 overexpression on miRNA-34b mimics-induced inhibition of RGC-5 cell proliferation (72 hours); (B) Annexin V-FITC/PI double staining detecting the reversal effect of TIA-1 overexpression on miRNA-34b mimics-induced apoptosis; (C) Flow cytometry detecting the reversal effect of TIA-1 overexpression on miRNA-34b mimics-induced G0/G1 phase arrest. Data are presented as mean ± standard deviation from three independent experiments. **P < 0.01 vs. NC mimics + empty vector; #P < 0.05 vs. miRNA-34b mimics + empty vector.

Therefore, the TIA-1-SG pathway may be only one component of the miRNA-34b regulatory network, rather than the sole pathway.

Compared with the known pathological mechanisms of NMOSD, AQP4 antibody-mediated complement-dependent cytotoxicity is the core driver of NMOSD (Chu *et al*., 2023). However, this study did not measure AQP4 antibody levels in serum or tissues, nor did it introduce AQP4 antibodies or complement into the cellular model to simulate the disease microenvironment, which is a major drawback. It remains unclear whether changes in miRNA-34b expression are correlated with AQP4 antibody titers, nor is it known whether miRNA-34 b's regulatory effects persist in the presence of AQP4 antibodies. Future studies should repeat these experiments in the presence of AQP4 antibody-positive serum or complement, and validate the in *vivo* function of miRNA-34b in animal models.

Although this study found that miRNA-34b inhibits cell proliferation and promotes apoptosis, there is insufficient evidence to use it directly as a diagnostic biomarker or therapeutic target for NMOSD. First, this study is purely in vitro and lacks *in vivo* pharmacodynamic data. Second, the sample size of this study was small, and receiver operating characteristic curve analysis was not performed to evaluate the diagnostic sensitivity and specificity of miRNA-34b. Third, the *in vivo* delivery efficiency of miRNA-34b mimics, their ability to cross the blood-brain barrier and their potential off-target effects have not been evaluated.

Cell model limitations and the need for validation in relevant cell types. The most significant limitation of this study is the exclusive use of the RGC-5 cell line. NMOSD is fundamentally an astrocytopathy, in which AQP4-IgG initiates complement-dependent cytotoxicity primarily in astrocytes, leading to secondary demyelination and neuronal injury. RGC-5 cells, being neuron-like, do not express AQP4 at levels sufficient to model the primary immunopathology of NMOSD. Furthermore, RGC-5 cells have been reported to exhibit phenotypic instability. Therefore, the observed effects of miR-34b on proliferation, apoptosis, and the TIA-1-SG pathway in this model cannot be directly extrapolated to astrocytes or oligodendrocytes, which are the primary targets of the disease. Consequently, this finding should be considered as preliminary mechanistic insights in a surrogate neuronal model. Future studies must replicate these experiments in more pathophysiologically relevant cell types, such as primary human astrocytes or AQP4-expressing astrocyte cell lines, preferably in the presence of patient-derived AQP4-IgG and complement.

CONCLUSION

In conclusion, this study demonstrates that miRNA-34b expression is downregulated in NMOSD lesional tissues and is associated with disease stage. In vitro functional

experiments showed that miRNA-34b negatively regulates the TIA-1-stress granule pathway by directly targeting the 3'-UTR of TIA-1 mRNA, thereby inhibiting RGC-5 cell proliferation, inducing G0/G1 phase arrest, and promoting cell apoptosis. Overexpression of TIA-1 partially reversed the above effects, suggesting that TIA-1 is a key downstream effector of miRNA-34b. However, this study has significant limitations, including being exclusively in vitro, limitations of the cell model, a small sample size, and a lack of in *vivo* validation. Therefore, these findings should be considered exploratory hypothesis-generating evidence rather than definitive mechanistic conclusions. The value of miRNA-34b as a potential biomarker or therapeutic target for NMOSD needs to be validated in more robust animal models and clinical samples. Future studies should prioritize the use of astrocyte cell models, repeat the functional experiments in the presence of AQP4 antibodies and complement and evaluate the *in-vivo* efficacy and safety of miRNA-34b mimics using NMOSD animal models.

Acknowledgments
We gratefully acknowledge the Lanzhou Petrochemical General Hospital for providing the necessary equipment for this study.

Authors' contributions
Yan Dai: Conceptualization, methodology, formal analysis, writing-original draft, supervision, funding acquisition; Yuhuan Liu: Investigation, validation, data curation, writing-review and editing; Anlang Dai: Resources, software, visualization, writing-review and editing. All authors have read and approved the final version of the manuscript.

Funding
There was no funding.

Data availability statement
The datasets generated during and/or analysed during the current study are available from the corresponding author on reasonable request.

Ethical approval
This study was approved by the Ethics Committee of Lanzhou Petrochemical General Hospital (Approval No.: SP-2025-258) and written informed consent was obtained from all patients or their guardians.

Conflict of interest
The authors declare no conflict of interest.

REFERENCES

Baymiller M, Helton NS, Dodd B and Moon SL (2026). tRNA synthetase activity is required for stress granule and P-body assembly. *Genes Dev.*, **40**(7-8): 475-497.

Chu F, Shi M, Liu C and Zhu J (2023). Discrepancy in clinical and laboratory profiles of NMOSD between AQP4 antibody positive and negative: Can NMOSD be diagnosed without AQP4 antibody? *Clin Exp Immunol*., **213**(3): 363-370.

Dalby B, Cates S, Harris A, Ohki EC, Tilkins ML, Price PJ and Ciccarone VC (2004). Advanced transfection with lipofectamine 2000 reagent: Primary neurons, siRNA and high-throughput applications. *Methods*., **33**(2): 95-103.

Han YH, Xing XY, Lee DH, Mao YY, Jin MH, Sun HN and Kwon T (2023). Induction of targeted differentiation of dermal mesenchymal stem cells into neural lineage according to peroxiredoxin II expression. *In-vivo*., **37**(4): 1593-1602.

Hsu JL, Su JJ, Cheng MY, Liao MF, Kuo HC, Chu CC, Chen CM, Chang KH, Chang CW, Wu YR, Huang CC, Bai CH and Ro LS (2025). Epidemiology and diagnostic challenges in neuromyelitis optica spectrum disorder in Taiwan: A hospital-based surveillance accompanied by a nationwide study. *Brain Commun*., **7**(4): 293.

Jiao D, Sun H, Zhao X, Chen Y, Lv Z, Shi Q, Li Y, Wang C and Gao K (2024). mTORC1/S6K1 signaling promotes sustained oncogenic translation through modulating CRL3IBTK-mediated ubiquitination of eIF4A1 in cancer cells. *Elife*., **12**: RP92236.

Jin Y, Chen Z, Liu X and Zhou X (2013). Evaluating the microRNA targeting sites by luciferase reporter gene assay. *Methods Mol Biol*., **936**: 117-127.

Kanai Y, Nishihara H, Miyagi Y, Tsuruyama T, Taguchi K, Katoh H, Takeuchi T, Gotoh M, Kuramoto J, Arai E, Ojima H, Shibuya A, Yoshida T, Akahane T, Kasajima R, Morita KI, Inazawa J, Sasaki T, Fukayama M and Oda Y (2018). The Japanese society of pathology guidelines on the handling of pathological tissue samples for genomic research: Standard operating procedures based on empirical analyses. *Pathol Int*., **68**(2): 63-90.

Khadka B, Bhattarai AM, Dhakal B, Karki A, Acharya A and Poudel R (2022). Seronegative neuromyelitis optica spectrum disorder with longitudinally extending transverse myelitis and optic neuritis: A case report. *Ann. Med. Surg. (Lond)*., **78**: 103757.

Krishnamoorthy RR, Agarwal P, Prasanna G, Vopat K, Lambert W, Sheedlo HJ, Pang IH, Shade D, Wordinger RJ, Yorio T, Clark AF and Agarwal N (2001). Characterization of a transformed rat retinal ganglion cell line. *Brain Res Mol Brain Res*., **86**(1-2): 1-12.

Lee J, Hong I, Lee C, Kim D, Kim S and Lee Y (2024). SNPs in microRNA seed region and impact of miR-375 in concurrent regulation of multiple lipid accumulation-related genes. *Sci Rep*., **14**(1): 10924.

Lesniczak-Staszak M, Pietras P, Rucinski M, Johnston R, Sowiński M andrzejewska M, Nowicki M, Gowin E, Lyons SM, Ivanov P and Szaflarski W (2024). Stress granule-mediated sequestration of EGR1 mRNAs

correlates with lomustine-induced cell death prevention. *J Cell Sci*., **137**(12): jcs261825.

Liu Q, Archilla I, Lopez-Prades S, Torres F, Camps J and Cuatrecasas M (2025). Polymorphic single-nucleotide variants in miRNA genes and the susceptibility to colorectal cancer: Combined evaluation by pairwise and network meta-analysis, thakkinstian's algorithm and FPRP criterium. *Cancer Med*., **14**(2): e70621.

Liu R, Chen J, Wang J, Zhang T, Xia Y, Feng J, Guo C, Xue L and Zhou Y (2026). Hepatocyte TIA1 constrains metabolic steatohepatitis by translationally suppressing Srebf1 mRNA in stress granules. *Cell Death Dis*., **17**(1): 357.

Lu X, Hu K, Zhang D, Yin X, Nie J and Zhao K (2024). KLF5 silencing restrains proliferation, invasion, migration and angiogenesis of gallbladder carcinoma cells by transcriptional regulation of PDGFA. *J Cancer Res Clin Oncol*., **151**(1): 11.

Ma H, Ou ZL, Alaeiilkhchi N, Cheng YQ, Chen K, Chen JY, Guo RQ, He MY, Tang SY, Zhang X, Huang ZP, Liu J, Liu J, Zhu QA, Huang ZC and Jiang H (2024). MiR-223 enhances lipophagy by suppressing CTSB in microglia following lysolecithin-induced demyelination in mice. *Lipids Health Dis*., **23**(1): 194.

McCreary M, Mealy MA, Wingerchuk DM, Levy M, DeSena A and Greenberg BM (2018). Updated diagnostic criteria for neuromyelitis optica spectrum disorder: Similar outcomes of previously separate cohorts. *Mult. Scler. J. Exp. Transl. Clin*., **4**(4): 2055217318815925.

McGurran H, Graceffo E, Kumbol V, Jendrach M, Hinkelmann L, Brehm M, Ravatt L, Krüger C, Wallach T, Haake A, Wegmann S, Heppner FL, Schülke M and Lehnardt S (2026). MicroRNA-29a-5p contributes to neuroinflammation through TLR7. *J Neuroinflammation*., **23**(1): 38.

Mohamed AS, Abdel-Fattah DS, Abdel-Aleem GA, El-Sheikh TF and Elbatch MM (2023). Biochemical study of the effect of mesenchymal stem cells-derived exosome versus L-Dopa in experimentally induced Parkinson's disease in rats. *Mol Cell Biochem*., **478**(12): 2795-2811.

Mosmann T (1983). Rapid colorimetric assay for cellular growth and survival: Application to proliferation and cytotoxicity assays. *J. Immunol. Methods*., **65**(1-2): 55-63.

Naki M, Gourdomichali O, Zonke K, Kattan FG, Makridakis M, Kontostathi G, Vlahou A and Doxakis E (2022). APEX2-mediated proximity labeling resolves the DDIT4-interacting proteome. *Int. J. Mol. Sci*., **23**(9): 5189.

Nicoletti I, Migliorati G, Pagliacci MC, Grignani F and Riccardi C (1991). A rapid and simple method for measuring thymocyte apoptosis by propidium iodide staining and flow cytometry. *J. Immunol. Methods*., **139**(2): 271-279.

Przybyszewski O, Mik M, Nowicki M, Kusinski M, Mikolajczyk-Solinska M and Sliwinska A (2024). Using microRNAs networks to understand pancreatic cancer-A literature review. *Biomedicines*., **12**(8): 1713.

Ramedani F, Jafari SM, Saghaeian Jazi M, Mohammadi Z and Asadi J (2023). Anti-cancer effect of entacaponeon esophageal cancer cells via apoptosis induction and cell cycle modulation. *Cancer Rep (Hoboken)*., **6**(3): e1759.

Ranga S, Yadav R, Chhabra R, Chauhan MB, Tanwar M, Yadav C, Kadian L and Ahuja P (2023). Long non-coding RNAs as critical regulators and novel targets in cervical cancer: Current status and future perspectives. *Apoptosis*., **28**(7-8): 925-942.

Sahin B, Bural IB, Ozcan H, Yildirim S, Tanriover G and Yoldas SB (2025). Association of miR-34a with metastatic progression through the FoxO3a-SIRT1 regulatory axis in breast cancer. *Turk. J. Med. Sci*., **56**(1): 326-332.

Sarkar S, Ganguly S, Ganguly NK, Sarkar DP and Sharma NR (2024). Chandipura virus forms cytoplasmic inclusion bodies through phase separation and proviral association of cellular protein kinase R and stress granule protein TIA-1. *Viruses*., **16**(7): 1027.

Shao F, Jiang W, Gao Q, Li B, Sun C, Wang Q, Chen Q, Sun B, Shen H, Zhu K, Zhang J and Liu C (2017). Frozen tissue preparation for high-resolution multiplex histological analyses of human brain specimens. *J. Neurooncol*., **135**(1): 21-28.

Vermes I, Haanen C, Steffens-Nakken H and Reutelingsperger C (1995). A novel assay for apoptosis. Flow cytometric detection of phosphatidylserine expression on early apoptotic cells using fluorescein labelled Annexin V. *J. Immunol Methods*., **184**(1): 39-51.

Zeng Y, Tang X, Chen J, Kang X and Bai D. (2024). Optimizing total RNA extraction method for human and mice samples. *Peer J*., **12**: e18072.